



HAL
open science

On the influence of the nozzle exhaust initial conditions on the near field acoustic pressure

Roberto Camussi, Stefano Meloni, Christophe Bogey

► **To cite this version:**

Roberto Camussi, Stefano Meloni, Christophe Bogey. On the influence of the nozzle exhaust initial conditions on the near field acoustic pressure. *Acta Acustica*, 2022, 6, 10.1051/aacus/2022051 . hal-03886262

HAL Id: hal-03886262

<https://hal.science/hal-03886262v1>


Submitted on 6 Dec 2022

HAL is a multi-disciplinary open access archive for the deposit and dissemination of scientific research documents, whether they are published or not. The documents may come from teaching and research institutions in France or abroad, or from public or private research centers.

L'archive ouverte pluridisciplinaire **HAL**, est destinée au dépôt et à la diffusion de documents scientifiques de niveau recherche, publiés ou non, émanant des établissements d'enseignement et de recherche français ou étrangers, des laboratoires publics ou privés.



On the influence of the nozzle exhaust initial conditions on the near field acoustic pressure

Roberto Camussi¹, Stefano Meloni^{1,2,*} , and Christophe Bogey³ 

¹Roma Tre University, Department of Engineering, Via Vito Volterra, 62, 00146 Rome, Italy

²Università della Tuscia, Department of Economics, Engineering, Society and Business Organization, 01100 Viterbo, Italy

³Univ Lyon, CNRS, Ecole Centrale de Lyon, INSA Lyon, Université Claude Bernard Lyon I, Laboratoire de Mécanique des Fluides et d'Acoustique, UMR 5509, 69134 Ecully, France

Received 29 April 2022, Accepted 10 November 2022

Abstract – In this paper, the acoustic pressure generated in the near field of a single stream cold jet is investigated. The analysis is focused on the effect of the initial conditions at the nozzle exit parametrized by considering two different turbulence levels and two different boundary layer thicknesses. The study has been performed by processing a numerical database obtained by large-eddy simulations (LES) of a jet flow at $M = 0.9$ and $Re = 10^5$. Pressure time series are obtained from pointwise virtual probes located in several radial and axial positions in the jet near-field. The acoustic pressure is extracted by the application of a consolidated wavelet-based procedure and the achieved acoustic signals are analyzed in terms of global quantities as well as by computing wavelet-reconstructed Fourier spectra. The results show that both the boundary-layer thickness and the turbulence level significantly affect the acoustic pressure in terms of its intensity and directivity whereas the distribution of energy in the frequency domain depends appreciably, only on the boundary-layer thickness.

Keywords: Wavelet, Jet-noise

1 Introduction

Many years of research activity in the field of jet noise initiated by the seminal paper of Lighthill [1] have demonstrated that the investigation of the region close to the jet stream is essential to improve the knowledge of the flow physics and to identify the relevant noise sources. In this framework, a key role is played by the state of the flow at the jet nozzle exit that is known to influence significantly both the aerodynamic and the acoustic properties of the jet.

The initial conditions can be clustered into five main parameters: Reynolds number (Re), Mach number (Ma), the shear layer momentum defined by the boundary layer (BL) thickness, the boundary layer velocity profile [2–5], and the turbulence intensity (TI) [6]. The parameters Re and Ma can be easily controlled both in experiments and numerical simulations whereas much more difficulties arise for the other quantities, mainly in experiments. As pointed out in [7], the initial flow state and the disturbance levels are connected with each other, they may vary from one facility to another and they are difficult to be tuned appropriately to reproduce full-scale conditions.

The interest into this subject motivated a large body of literature dealing with both shear layers and compressible jets (see e.g. the early reviews by Crighton [8] and Gutmark and Ho [9]). To the extent of the jet cases, the literature about experiments is scarce, because of the difficulties in changing the inflow parameters independently [10]. On the other hand, several numerical studies were performed mainly with the scope of distinguishing the influence of the jet inflow parameters on the aerodynamic properties and the far-field noise [2, 3, 6].

As was suggested in [11], low turbulence or initially laminar jets emit additional noise components as an effect of the vortex pairing, recognized as an efficient noise generation mechanism. Bogey et al. [7] showed numerically that the sensitivity of the sound fields to the jet exit boundary layer conditions is larger in the transverse direction than in the downstream one. These results were in agreement with experimental data presented in [12, 13] where the noise emitted by tripped and un-tripped jets was investigated. Karon and Ahuja [14] found that a jet cexhausting from nozzles designed to reduce the axial velocity variation and the turbulence intensity, produces more noise compared to a nozzle with a fully developed flow at the exit. Furthermore, as speculated by Zaman [5], an increase of turbulence intensity in the initial

*Corresponding author: stefano.meloni@uniroma3.it

region of the jet shear layer leads to an increase of high-frequency noise.

Despite the large body of literature on the subject, the evaluation and prediction of the effects of the initial conditions on the generation and propagation of acoustic waves in compressible jets is still unclear. The present study tries to give a contribution to shed light on this complex issue by analyzing parametrically the pressure field in the near region of compressible subsonic jets. The knowledge of the near field pressure can explicate the process underlying the origin of the acoustic waves propagating to the far field. As pointed out in [15], the near field contains the beginnings of a sound field which is destined to reach the far field and the parametric analysis proposed therein attempts to clarify its sensitivity upon the initial conditions.

The data analyzed have been obtained by LES already presented in [7, 16, 17]. The data set covers a domain that varies in the streamwise direction from $x/D = 0$ up to $x/D = 20$ and in the radial direction from the nozzle lip ($r/D = 0.5$) up to $r/D = 3$, by denoting with D the jet exit diameter.

Two different turbulence intensities and boundary layer thickness are considered by keeping fixed the exhaust Reynolds number and the jet Mach number. The influence of these parameters on the aerodynamic properties of the same jet was presented in [3].

As pointed out in several previous papers [15, 18–20], the near field pressure contains both hydrodynamic (pseudo-sound) and acoustic components that have to be analyzed separately. In the present investigation, the separation is achieved by the application of a procedure based on the wavelet transform, that is briefly worked out in the following section. This section also clarifies which are the statistical quantities extracted from the pressure data and the results of these analyses are presented in Section 3. The main conclusions and final remarks are eventually given in Section 4.

2 Numerical setup and postprocessing procedure

2.1 Numerical setup

The database analyzed has been obtained numerically through LES of four isothermal single stream cold circular jets, operating at $Ma = 0.9$ and $Re = 10^5$. The LES are performed using grids containing between 250 million and 1 billion points with low-dissipation schemes and relaxation filtering as a subgrid dissipation model, see [21] for the details. In the first two cases, the values of the exit peak turbulence intensities (TI) have been fixed at 3% and 9% by numerically tripping the boundary layers in the pipe and by adding random low-level vortical disturbances decorrelated in the azimuthal direction. In the two other cases, the BL are untripped yielding $TI = 0$. The second couple of parameter is the boundary layer thickness (δ) which has been varied from 0.0025 up to 0.02 times the jet radius, having a laminar Blasius velocity profile. The jet initial conditions of the presented data have been resumed in Table 1.

Table 1. Jet initial conditions.

M	Re_D	TI	δ/r_0
0.9	10^5	3%	0.15
0.9	10^5	9%	0.15
0.9	10^5	0	0.025
0.9	10^5	0	0.2

The LES are performed using a solver of the three-dimensional filtered compressible Navier–Stokes equations using low-dissipation and low-dispersion finite differences developed in [22]. The quality of the shear-layer discretization was assessed in [17].

The spatial domain of the simulation is $15r_0$ long in the radial direction and $40r_0$ long in the axial direction, by denoting with r_0 the nozzle exhaust radius. The mesh size in the considered domain varies between $0.72 < \Delta r/r_0$ (%) < 2.48 in the radial direction and $1.452 < \Delta x/r_0$ (%) < 2.49 in the axial direction (see [3, 16, 23] for further details). The time step is defined by $\Delta t = 0.7\Delta r(r = r_0)/ca$, yielding $\Delta t = 0.0023r_0/u_j$ where u_j is the jet exit velocity. After the transient period, data have been recorded for a simulation time T equal to or higher than $500r_0/u_j$, at a sampling frequency yielding a maximum Strouhal number $St_D = fD/u_j = 6.4$, where f is the frequency [23].

The present study is limited to the near-field domain, usually recognized as the noise-producing region of the jet flow and thus of interest for jet–noise modeling. Pressure time series are extracted from virtual probes at different locations in the near field, covering a domain that spans from the nozzle exhaust up to $x/D = 20$ in the axial direction and from the nozzle lip line ($r/D = 0.5$) up to $r/D = 3$ in the radial one.

2.2 Wavelet-based post-processing procedures

The present study is targeted to the analysis of the near field pressure and a crucial step of the data processing relies on the separation of the acoustic component of the pressure signals from the hydrodynamic one. This goal is achieved by the application of a procedure proposed by [18, 20] that is briefly worked out in the following.

The method is based on the wavelet transform of the given signals and by an appropriate filtering of the resulting wavelet coefficients. It is known that the wavelet transform is a very proficient tool when it comes to analyzing intermittent or time-dependent features. When considering pressure time series $p(t)$, the wavelet transform can be formally represented by the following expression [24–28]:

$$w(s, t) = C_\psi^{-\frac{1}{2}} s^{-\frac{1}{2}} \int_{-\infty}^{\infty} p(\tau) \psi^* \left(\frac{t-\tau}{s} \right) d\tau, \quad (1)$$

where s is the wavelet scale, τ is a time shift, $C_\psi^{-\frac{1}{2}}$ is a constant that takes into account the mean value of $\psi(t)$ and $\psi^* \left(\frac{t-\tau}{s} \right)$ is the complex conjugate of the dilated and translated mother wavelet $\psi(t)$. In the present approach, the Morlet wavelet kernel has been adopted but, as was shown in [18], the results are independent from the choice

of the wavelet type. A series of wavelet coefficients, characterized by different amplitudes, and distributed into a time-frequency domain, were obtained after applying equation (1). Once passed into the wavelet domain, various separation techniques can be used to extract the quantities of interest. According to the literature, [18, 25], the acoustic/hydrodynamic separation algorithms assume that the hydrodynamic contribution is related to localized eddy structures that compresses well onto the wavelet basis so that it can be described by a few but with large amplitude wavelet coefficients. Thus, the so-called pseudo-sound (i.e., the hydrodynamic component of pressure fluctuations) can be extracted by selecting the wavelet coefficients exceeding a proper threshold. The acoustic counterpart associated with more homogeneous and lower energy fluctuations is represented by those coefficients having an amplitude lower than the threshold [25]. The selection of the threshold level represents a crucial step in the separation procedure and several approaches have been proposed in literature [25]. The method applied in the present work is the so-called WT3, which is a very fast separation procedure based on single-point statistics. In this method, the threshold varies iteratively starting from an initial guess evaluated according to the following formula

$$T = \sqrt{\sigma_{\|k} \log_{10} N_s}, \quad (2)$$

where σ is the variance of the (presumed) acoustic pressure at iteration k and N_s is the number of samples. The algorithm stops when the number of selected acoustic wavelet coefficients remains constant between two consecutive iterations. The method has been successfully applied and validated in several previous papers including configurations significantly different from the one analyzed therein (see e.g. [29–32]).

In the present approach, the application of the decomposition procedure provides the reconstruction in the physical domain of the acoustic pressure in the near field of the jet. The pressure time series are eventually analyzed to extract the relevant quantities needed to evaluate the effect of the conditions at the nozzle exit.

To the extent of the noise level estimations, the most relevant indicator is the Overall Sound Pressure Level (OASPL) defined as follows:

$$\text{OASPL} = 10 \log_{10} \left(\frac{\sigma^2}{P_{\text{ref}}^2} \right), \quad (3)$$

where σ is the standard deviation of the pressure signal and P_{ref} is the reference pressure in air (equal to 20 μPa).

A more detailed estimation of the influence of the initial conditions can be retrieved by the analysis in the frequency domain through the computation of the Fourier Power Spectral Density (PSD) of the pressure signals. However, as usually experienced in numerical simulations, the number of available samples is limited, this drawback affecting significantly the statistical convergence and thus the reliability of the PSD.

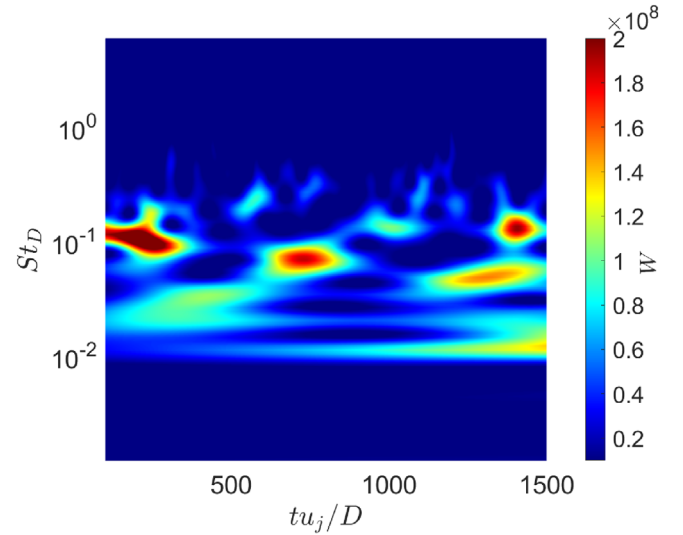


Figure 1. A wavelet scalogram computed from a signal taken at $\text{TI} = 9\%$, $r/D = 3$ and $x/D = 10$.

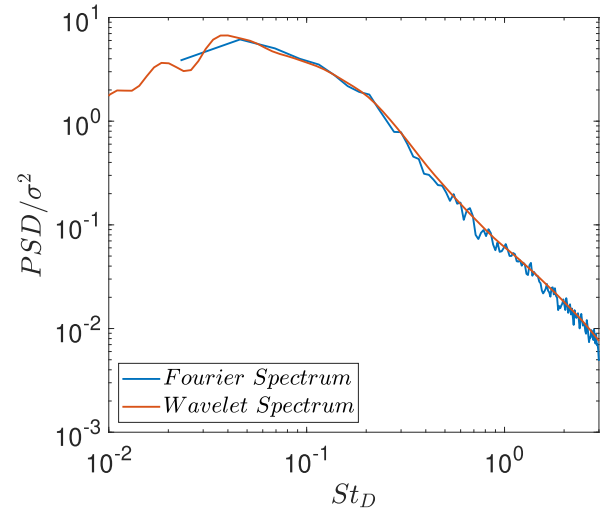


Figure 2. Comparison between a Fourier Power Spectrum (dotted line) and the corresponding wavelet-reconstructed Fourier Spectrum (solid line). Data are taken at $\text{TI} = 9\%$, $r/D = 3$ and $x/D = 10$.

In order to overcome this flaw, it is possible to reconstruct the Fourier PSD by performing the wavelet transform of the signals and by integrating the so-called scalogram [33]. This quantity is obtained by the square of the wavelet coefficients and represents a projection onto the 2D time-frequency domain of the energy contained by the signal [34]. An illustrative example of the wavelet scalogram obtained by processing a segment of an acoustic pressure signal is reported in Figure 1. The wavelet scalogram shows energetic events appearing intermittently in time at low St_D . These signatures could be ascribed to the passage of the large scales flow structures, which characterize the turbulent jet downstream of the end of the potential core.

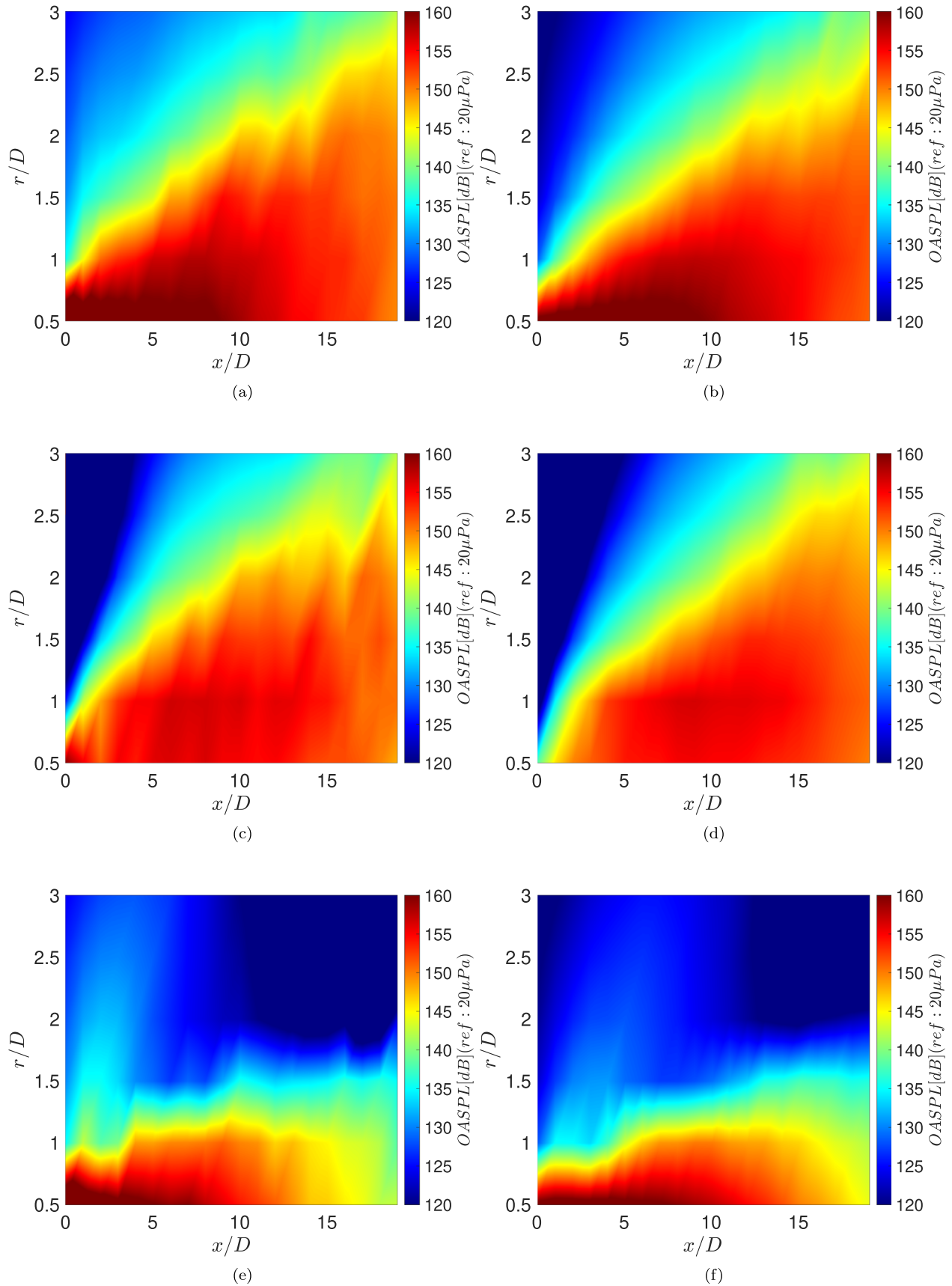


Figure 3. ASPL contour maps for TI = 3% (a, c, e) and TI = 9% (b, d, f): (a) and (b) original signals; (c) and (d) hydrodynamic components; (e) and (f) acoustic components.

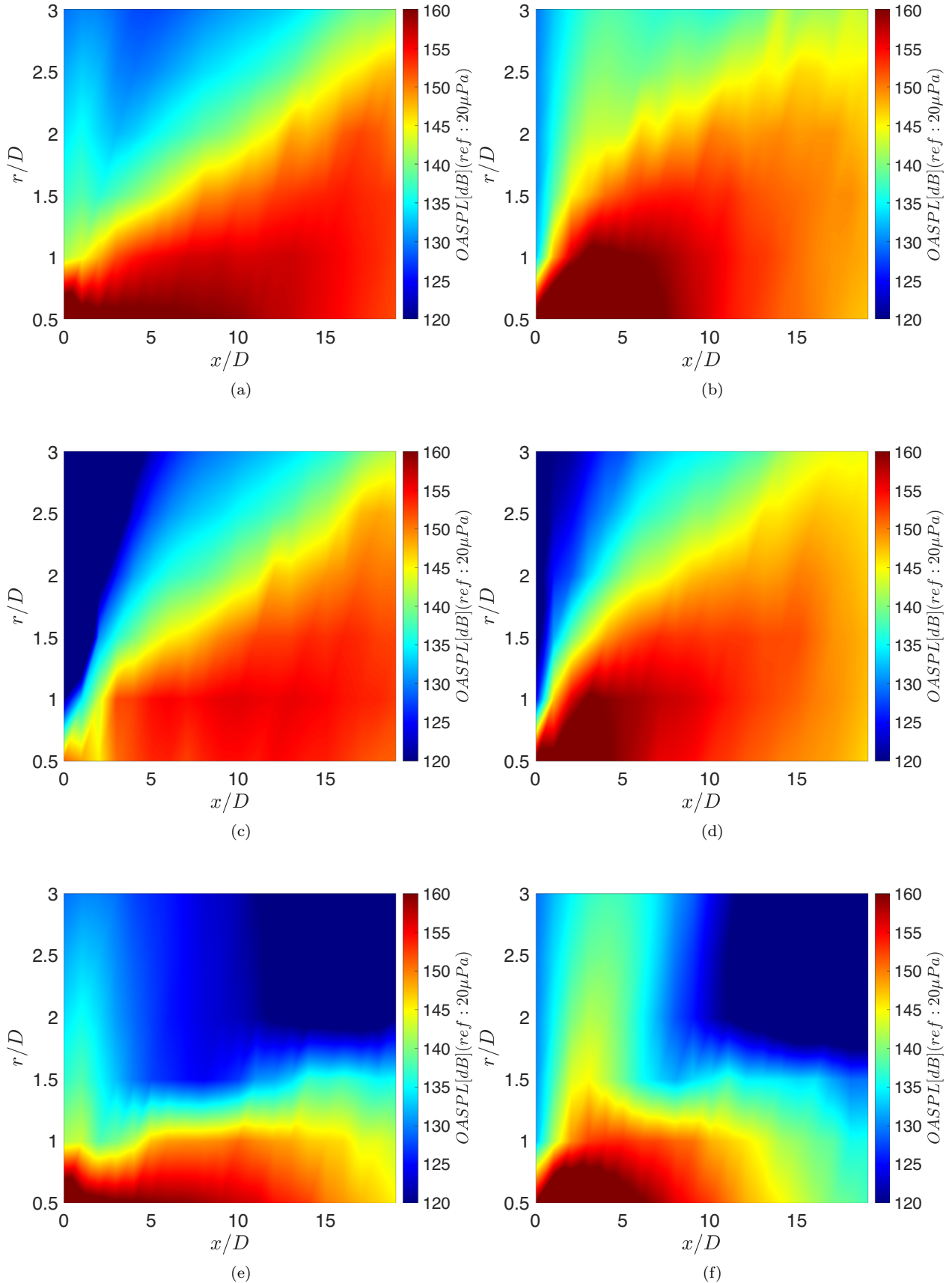


Figure 4. OASPL contour maps for $\delta = 0.025$ (a, c, e) and $\delta = 0.2$ (b, d, f): (a) and (b) original signals; (c) and (d) hydrodynamic components; (e) and (f) acoustic components.

The integral in time of the wavelet scalogram provides the Fourier spectrum. The capability of the wavelet-reconstructed Fourier spectrum to be statistically more effective than the standard Fourier one was already recognized in the seminal paper by Farge [28] where it is emphasized that the global wavelet energy spectrum corresponds to the Fourier energy spectrum smoothed by the wavelet spectrum at each scale. An example of a comparison between the Fourier and the wavelet-reconstructed spectrum is provided in Figure 2 showing a very good agreement. The wavelet spectrum looks less noisy and better defined at any St_D . This procedure will then be adopted in the analyses presented below.

3 Results

An overall picture of noise emitted in the different nozzle exhaust configurations is presented through the contour plots of the OASPL. Figure 3 reports the effect of the turbulence intensity (TI), on the original (first row), hydrodynamic (second row) and acoustic (third row) pressure. The left column corresponds to TI = 3% and the right one to TI = 9%. According to [18], the original and hydrodynamic pressure distributions look very similar whereas the acoustic pressure appears more localized around the jet potential core. Furthermore, for both the two TI considered, a stronger directivity of the acoustic pressure towards the sideline, at about 90° that corresponds to x/D close to 0, is observed.

This directivity effect is even more evident when the laminar cases are analyzed, as reported in Figure 4. In this case, the column on the left corresponds to the smallest boundary layer thickness. Again, the original and hydrodynamic pressure distributions are very similar to each other whereas the acoustic one is more localized. It is interesting to note that the case with the acoustic pressure for largest thickness (case 4f) is concentrated within the potential core. A lower thickness (case 4e) leads to a spreading of the intensity along x/D and a lower intensity of the pressure in the 90° direction. It is supposed that for smaller boundary layer thickness, the shear layer tends to be more unstable and thus to destabilize rapidly reaching a turbulence state after a few diameters downstream of the nozzle exit. On the other hand, for a thinner boundary layer, the shear layer persists up to more than 10 diameters.

The evolution of the OASPL with x/D is presented in more details in Figure 5. The case 5a reports the effect of the turbulence level whereas the effect of the boundary layer thickness is presented in case 5b. For each case, the OASPL is presented as a function of x/D for two the radial positions, $r/D = 0.5$ and 3.

To the extent of the TI effect (Fig. 5a) it is very interesting to note that the noise generated in the case at lower TI is larger at low x/D , corresponding to the stronger directivity at around 90° observed above. The noise level decreases for increasing x/D , independently from TI but, at very large x/D , the case with higher TI becomes noisier. A possible interpretation can be provided by considering

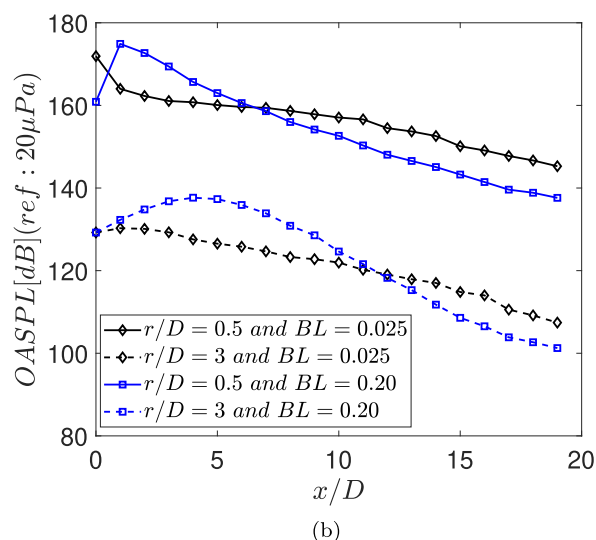
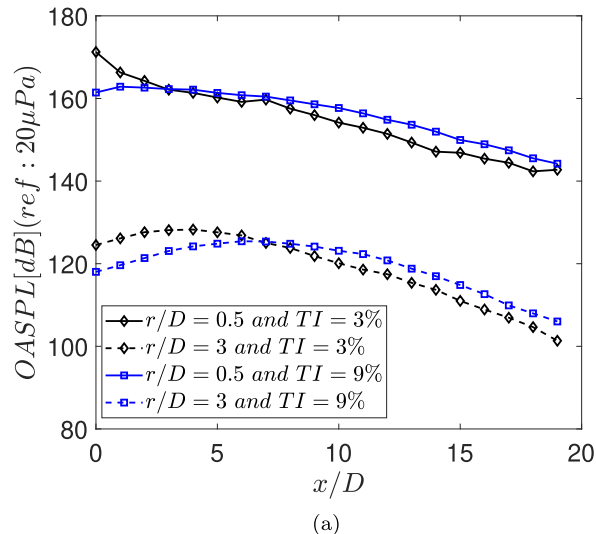


Figure 5. OASPL axial evolution at radial locations $0.5D$ and $3D$: (a) different TI and (b) different δ .

the concept of similarity spectra introduced by Tam [35]. The directivity around 90° is dominated by the noise from the fine scale of turbulence whereas at larger angles, corresponding to larger x/D , noise is dominated by acoustic waves radiated by the large-scale structures. The result presented in Figure 5a shows that at low TI, noise generated by the small scale structures is more effective due to the formation and pairing of vortical structures near the jet nozzle, whereas the larger TI induces the larger scales to be more efficient noise sources and to dominate at larger x/D .

A similar interpretation can be assumed to explain the effect of the boundary-layer thickness, reported in Figure 5b. Surprisingly, the case with a larger thickness, except for $x/D = 0$, emits noise more efficiently at low x/D , corresponding to the directivity close to 90° . The boundary layer with larger thickness is therefore more efficient in terms of noise generated by small scale structures, because those small coherent structures persist over a large axial distance.

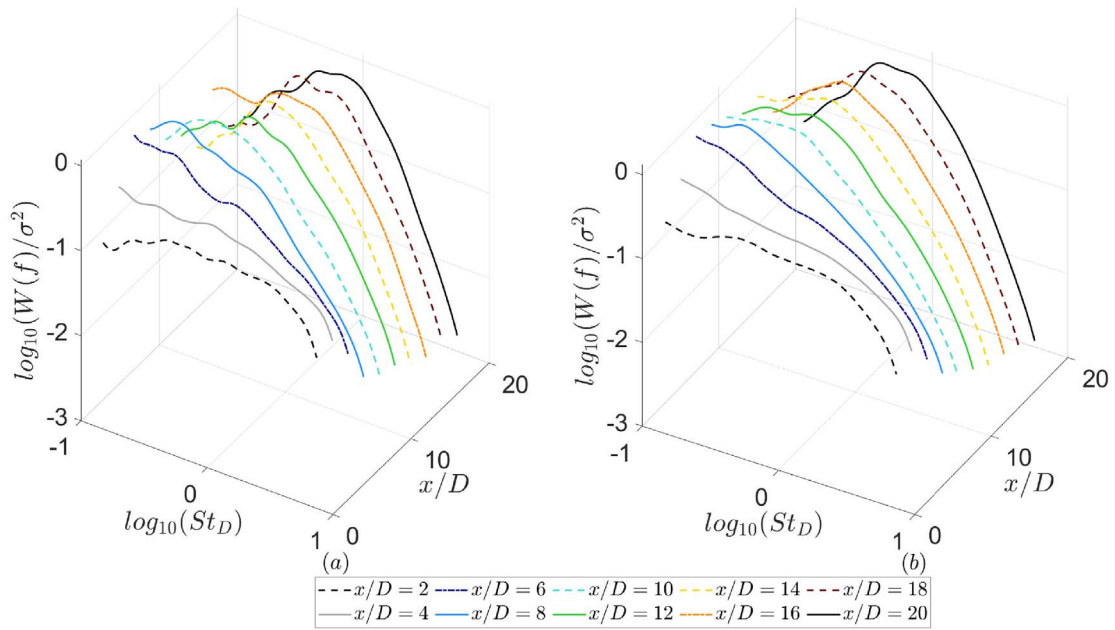


Figure 6. Wavelet spectra taken at $r/D = 3$ for different x/D and different TI: (a) TI = 3% and (b) TI = 9%.

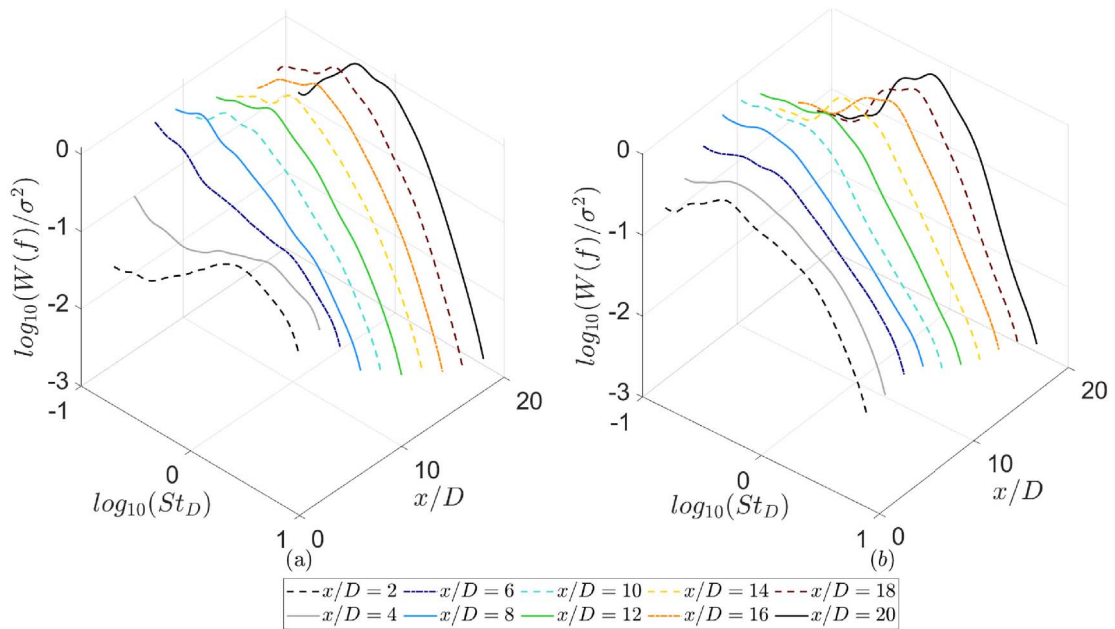


Figure 7. Wavelet spectra taken at $r/D = 3$ for different x/D and different boundary layer thickness d . (a) $\delta/D = 0.0025$ and (b) $\delta/D = 0.02$.

For increasing x/D , independently from r/D , the case with thinner boundary layer becomes dominant as an increasing effect of the large scale noise that is relevant at large directivity angles (according to [35], the directivity angle is conventionally assumed to increase from the sideline at 90° towards the jet flow direction, thus towards increasing x/D).

In summary, in the direction of the jet maximum directivity, at about 150° corresponding to large x/D , the jets with larger TI and lower BL thickness generate more noise.

On the other hand, at low directivity angles, around 90° corresponding to small x/D , the trend is the opposite: the largest noise emission is observed for low TI and large BL thickness.

The analysis in the Fourier domain can support the physical interpretations and highlight the distribution of energy at the different scales. The Wavelet-reconstructed Fourier spectra obtained at the two TI are presented in Figure 6 whereas the effect of the boundary layer thickness is given in Figure 7.

The spectra are reported for different x/D and are all normalized with respect to the corresponding variance. In this way, the amplitude variations are compensated and the energy distribution among different frequencies is better highlighted.

The cases reported in [Figure 6](#) show that the acoustic energy moves from high frequencies at low x/D to lower frequencies moving far from the jet exit. The energy bump at large x/D corresponds to a St_D of about 0.5 that reflects the trace of the Kelvin–Helmholtz instability mode. The effect of the TI level seems to be weak since the shape of the spectra are similar except for a smoother behavior in the case of larger TI ([Fig. 6b](#)). This result varies in agreement with a previous paper [7], where the influence of the nozzle exit turbulence on the velocity spectra has been characterized, observing similar spectral shapes but with different energy content for the two considered cases.

A similar evolution is observed in [Figure 7](#) where the cases corresponding to laminar conditions and different boundary layer thickness are reported. The thinner boundary layer ([Fig. 7a](#)) exhibits a clear bump at high frequencies, very probably as an effect of the small size of the boundary layer thickness. This bump is not present in the case with thicker boundary layer where the energy at small x/D is large at much lower frequencies. This is probably an effect of the larger size of the boundary layer thickness which induces a slower development of the mixing layer. According to [3] the shear-layer transition is smoother in the jets with thicker exit boundary layers. Also in this case, moving towards larger x/D , the energy tends to concentrate around the Kelvin–Helmholtz frequency.

4 Conclusions

This paper reports an analysis of the influence of the conditions at the nozzle exit of a compressible subsonic jet on the near field acoustic pressure. The investigation is carried out by processing a numerical data-base obtained by well resolved LES at fixed Mach and Reynolds numbers. The properties at the nozzle exit presently investigated consist of the turbulence level and the boundary layer thickness. Two values of each parameter are considered and the response of the pressure field is evaluated by analyzing pressure time series taken from virtual probes distributed in a region covering up to $x/D = 20$ in the streamwise direction and $r/D = 3$ in the radial one. The two TIs are obtained at constant boundary layer thickness, whereas the two cases with different thickness correspond to laminar conditions. A key role in the data processing procedures is played by the wavelet transform that is used to extract the acoustic component of the pressure fluctuations that, being in the near field, is combined with the hydrodynamic counterpart. The separation is achieved by the application of an existing wavelet-based procedure that relies on the application of an iterative process that converges rapidly. Wavelet analysis is adopted also to estimate accurately the frequency spectra. Indeed, due to the limited number of samples, the standard Welch method commonly used for the computation of the

PSDs is not sufficiently reliable in terms of statistical convergence. On the other hand, the reconstruction of the Fourier spectra by the integration of the wavelet scalogram, is shown to be much more effective.

The distribution of the OASPL gives an overall indication of the effects of the two parameters analyzed. As opposed to the original and hydrodynamic pressure, the acoustic pressure component exhibits a stronger OASPL increasing towards the sideline, this effect being more relevant at the lowest turbulence level. It is in fact very clear in the laminar cases and more pronounced for the thicker boundary layer. The strong directivity in the transversal direction can be ascribed to the generation of acoustic waves by small scale structures that apparently are more effective when the turbulence level is low. In the laminar case it is argued that the small scale vortices generated in the thicker boundary layer case persist over a larger axial distance and thus are more efficient in emitting noise in the side line direction. These conclusions are confirmed by the analysis of the evolution of the OASPL along x/D . It is shown that in the region close to the nozzle exit, corresponding to low directivity angles, the cases at low TI and thicker boundary layer are the noisiest. In all cases, the OASPL intensity decreases for increasing x/D and at large x/D , corresponding to large directivity angles, the larger TI and thinner boundary layer becomes dominant in terms of noise level.

The acoustic pressure PSDs show that, in all cases, in the region far from the nozzle exit, the energy is concentrated around the Kelvin–Helmholtz mode. The PSD shapes in the turbulent cases are shown to be weakly sensitive upon the TI levels whereas the dependence on the boundary layer thickness is more pronounced. Specifically, in the region very close to the nozzle exit, the case corresponding to the thinner boundary layer exhibit a relevant energetic content at high frequencies that, for increasing x/D , is redistributed towards lower frequencies. On the other hand, in the thicker case, the energy at low x/D is concentrated at smaller frequencies. This behaviour is probably related to the effect of the dominant length scales that, apparently, are smaller for the thinner case with respect to the thicker one.

Further studies are definitely needed to better establish and predict the influence of the initial conditions on the acoustic radiation. This challenging task can be pursued in the future by improving the parametric study and thus by increasing considerably the number of analyzed cases.

Conflict of interest

The authors declare no conflict of interest.

Acknowledgments

C. Bogey was partially supported by the LABEX CeLyA (ANR-10-LABX-0060/ANR-16-IDEX-0005).

The numerical data analyzed in this work were obtained using the HPC resources of PMCS2I (Pôle de Modélisation et de Calcul en Sciences de l'Ingénieur et de l'Information) of Ecole Centrale de Lyon and P2CHPD (Pôle de Calcul Hautes Performances Dédié) of Université Lyon I, and the resources of CINES (Centre Informatique National de l'Enseignement Supérieur) and IDRIS (Institut du Développement et des Ressources en Informatique Scientifique) under the allocation 2021-2a0204 made by GENCI (Grand Equipement National de Calcul Intensif).

References

1. M.J. Lighthill: On sound generated aerodynamically. General theory. *Proceedings of the Royal Society of London* 211 (1952) 564–587.
2. C. Bogey, R. Sabatini: Effects of nozzle-exit boundary-layer profile on the initial shear-layer instability, flow field and noise of subsonic jets. *Journal of Fluid Mechanics* 876 (2019) 288–325.
3. C. Bogey, O. Marsden: Identification of the effects of the nozzle-exit boundary-layer thickness and its corresponding reynolds number in initially highly disturbed subsonic jets. *Physics of Fluids* 25, 5 (2013) 055106.
4. C. Bogey: Generation of excess noise by jets with highly disturbed laminar boundary-layer profiles. *AIAA Journal* 59, 2 (2021) 569–579.
5. K.B.M.Q. Zaman: Increased jet noise due to a “nominally laminar” state of nozzle exit boundary layer, in NASA Report, 2017.
6. C. Bogey, C. Bailly: Influence of nozzle-exit boundary-layer conditions on the flow and acoustic fields of initially laminar jets. *Journal of Fluid Mechanics* 663 (2010) 507–538.
7. C. Bogey, O. Marsden, C. Bailly: Influence of initial turbulence level on the flow and sound fields of a subsonic jet at a diameter-based reynolds number of 10^5 . *Journal of Fluid Mechanics* 701 (2012) 352–385.
8. D.G. Crighton: Acoustics as a branch of fluid mechanics. *Journal of Fluid Mechanics* 106 (1981) 261–298.
9. E. Gutmark, C.M. Ho: Preferred modes and the spreading rates of jets. *The Physics of Fluids* 26, 10 (1983) 2932–2938.
10. Z.D. Husain, A.K. Hussain: Axisymmetric mixing layer: influence of the initial and boundary conditions. *AIAA Journal* 17, 1 (1979) 48–55.
11. L. Maestrello, E. McDavid: Acoustic characteristics of a high-subsonic jet. *AIAA Journal* 9, 6 (1971) 1058–1066.
12. K.B.M.Q. Zaman: Effect of initial condition on subsonic jet noise. *AIAA Journal* 23, 9 (1985) 1370–1373.
13. J.E. Bridges, A.K. Hussain: Roles of initial condition and vortex pairing in jet noise. *Journal of Sound and Vibration* 117, 2 (1987) 289–311.
14. A.Z. Karon, K.K. Ahuja: Role of nozzle-exit boundary layer in producing jet noise. *International Journal of Aeroacoustics* 21 (2022) 626–653.
15. C.E. Tinney, P. Jordan: The near pressure field of co-axial subsonic jets. *Journal of Fluid Mechanics* 611 (2008) 175–204.
16. C. Bogey: Acoustic tones in the near-nozzle region of jets: characteristics and variations between mach numbers 0.5 and 2. *Journal of Fluid Mechanics* 921 (2021) A3.
17. C. Bogey: Grid sensitivity of flow field and noise of high-reynolds-number jets computed by large-eddy simulation. *International Journal of Aeroacoustics* 17, 4–5 (2018) 399–424.
18. M. Mancinelli, T. Pagliaroli, A. Di Marco, R. Camussi, T. Castelain: Wavelet decomposition of hydrodynamic and acoustic pressures in the near field of the jet. *Journal of Fluid Mechanics* 813 (2017) 716–749.
19. R.E.A. Arndt, D.F. Long, M.N. Glauser: The proper orthogonal decomposition of pressure fluctuations surrounding a turbulent jet. *Journal of Fluid Mechanics* 340 (1997) 1–33.
20. S. Grizzi, R. Camussi: Wavelet analysis of near-field pressure fluctuations generated by a subsonic jet. *Journal of Fluid Mechanics* 698 (2012) 93–124.
21. C. Bogey, O. Marsden, C. Bailly: Large-eddy simulation of the flow and acoustic fields of a reynolds number 10^5 subsonic jet with tripped exit boundary layers. *Physics of Fluids* 23 (2011) 035104.
22. C. Bogey, C. Bailly: A family of low dispersive and low dissipative explicit schemes for flow and noise computations. *Journal of Computational physics* 194, 1 (2004) 194–214.
23. C. Bogey: A database of flow and near pressure field signals obtained for subsonic and nearly ideally expanded supersonic free jets using large-eddy simulations. 2022.
24. S. Meloni, J.L.T. Lawrence, A.R. Proença, R.H. Self, R. Camussi: Wall pressure fluctuations induced by a single stream jet over a semi-finite plate. *International Journal of Aeroacoustics* 19, 3–5 (2020) 240–253.
25. R. Camussi, S. Meloni: On the application of wavelet transform in jet aeroacoustics. *Fluids* 6, 8 (2021) 299.
26. R. Camussi, G. Robert, M.C. Jacob: Cross-wavelet analysis of wall pressure fluctuations beneath incompressible turbulent boundary layers. *Journal of Fluid Mechanics* 617 (2008) 11–30.
27. S. Meloni, H. Kamliya Jawahar: A wavelet-based time-frequency analysis on the supersonic jet noise features with chevrons. *Fluids* 7, 3 (2022) 108.
28. M. Farge: Wavelet transforms and their applications to turbulence. *Annual Review of Fluid Mechanics* 24, 1 (1992) 395–458.
29. S. Li, D.E. Rival, X. Wu: Sound source and pseudo-sound in the near field of a circular cylinder in subsonic conditions. *Journal of Fluid Mechanics* 919 (2021) A43.
30. A. Hajczak, L. Sanders, F. Vuillot, P. Druault: Wavelet-based separation methods assessment on the near pressure field of a landing gear subcomponent, in 25th AIAA/CEAS Aeroacoustics Conference, 2019, p. 2482.
31. C. Pérez Arroyo, G. Daviller, G. Puigt, C. Airiau, S. Moreau: Identification of temporal and spatial signatures of broadband shock-associated noise. *Shock Waves* 29, 1 (2019) 117–134.
32. M. Mancinelli, A. Di Marco, R. Camussi: Multivariate and conditioned statistics of velocity and wall pressure fluctuations induced by a jet interacting with a flat plate. *Journal of Fluid Mechanics* 823 (2017) 134–165.
33. G.L. Micci, R. Camussi, S. Meloni, C. Bogey: Intermittency and stochastic modeling of low- and high-reynolds-number compressible jets. *AIAA Journal* 60, 3 (2022) 1983–1990.
34. G. Guj, R. Camussi: Statistical analysis of local turbulent energy fluctuations. *Journal of Fluid Mechanics* 382 (1999) 1–26
35. C.K.W. Tam: Supersonic jet noise. *Annual Review of Fluid Mechanics* 27, 2–3 (1995) 17–43.